Water Resources Research

RESEARCH ARTICLE
10.1029/2024WR039219

High Resolution Mapping of Submerged Sediment Size and Suitable Salmon Spawning Habitat Using Topo-Bathymetric Lidar in the Santiam River Basin, Oregon

James S. White[1], **Karen Bartelt**[1], **Brandon T. Overstreet**[1], **and Jake R. Kelley**[2]

[1]U.S. Geological Survey, Oregon Water Science Center, Portland, OR, USA, [2]U.S. Geological Survey, Western Fisheries Research Center, Cook, WA, USA

Key Points:

- River-bed sediment size is a driver of ecological and geomorphic processes but is difficult to characterize at high resolution over large areas
- Using bathymetric Lidar data to relate streambed roughness with georeferenced pebble counts provides a surrogate approach to quantifying bed sediment size
- This method was used to map bed sediment size, and subsequently suitable Chinook salmon spawning sediment, across 260 km of diverse rivers

Supporting Information:

Supporting Information may be found in the online version of this article.

Correspondence to:

J. S. White,
jameswhite@usgs.gov

Citation:

White, J. S., Bartelt, K., Overstreet, B. T., & Kelley, J. R. (2025). High resolution mapping of submerged sediment size and suitable salmon spawning habitat using topo-bathymetric Lidar in the Santiam River basin, Oregon. *Water Resources Research*, *61*, e2024WR039219. https://doi.org/10.1029/2024WR039219

Received 22 OCT 2024
Accepted 25 JUN 2025

Author Contributions:

Conceptualization: James S. White, Karen Bartelt, Brandon T. Overstreet
Formal analysis: James S. White, Karen Bartelt
Funding acquisition: James S. White, Brandon T. Overstreet
Methodology: James S. White, Karen Bartelt, Brandon T. Overstreet
Visualization: James S. White, Karen Bartelt, Jake R. Kelley
Writing – original draft: James S. White, Karen Bartelt, Jake R. Kelley

Abstract The distribution of river-bed grain sizes plays a foundational role in river morphology and ecology. River-bed grain size is a key driver of channel form and process, and has first order effects on aquatic macroinvertebrate assemblages, fish nesting, and biogeochemical processes. Despite this importance, tools to spatially quantify grain-size distributions, particularly submerged grain-size distributions, are lacking. Efforts to address this knowledge gap include developing optical and sonographic tools, however, these approaches have limitations, especially in shallow rivers and over large spatial extents. This study quantifies submerged grain size at high resolution (1 m^2) across 260 km of geomorphically diverse river corridors in the Santiam River Basin, Oregon, by pairing bathymetric Lidar point clouds with georeferenced pebble counts. Results suggest that derivatives of Lidar point clouds are able to accurately estimate measured median grain size across seven of the eight river reaches investigated, including reaches above and below high-head dams. Spatial analysis of predicted grain-sizes in the context of Chinook salmon spawning habitat suggests that suitable size sediment patches in the upper, unregulated reaches the study basin is typically small and unorganized. In contrast, the larger rivers downstream of high-head dams typically have larger areas of suitable spawning gravels. This method may be useful for quantification of fish and macroinvertebrates habitats, surface grain-size metrics for sediment transport models, and monitoring of natural and anthropogenic changes in river systems.

Plain Language Summary The nature of the sediment cover on the bed of a river helps determine what form that river takes and what types of flora and fauna can live within it. However, measuring and mapping the size of river-bed sediment is challenging, especially creating detailed maps of underwater sediment across large distances. This work uses specialized Lidar data collected from a crewed fixed-wing aircraft paired with field measurements of underwater river-bed sediment size to create detailed maps of grain size across 260 km of river. The resulting data were then used to map where in these there is sediment that is suitable for Chinook salmon to spawn. Results show this method reliably replicates ground-based measurements across a range of stream conditions and that the distribution of spawning habitat above and below dams is notably different.

1. Introduction

The distribution of surficial grain size plays a foundational role in physical and ecological riverine processes. Grain-size distributions influence channel morphology (Dade, 2000), hyporheic exchange (Tonina & Buffington, 2009), and hydraulic roughness (Buffington & Montgomery, 1999b). Ecologically, river-bed sediments provide the medium for fostering algal (Schneck et al., 2011) and macroinvertebrate communities (Erman & Erman, 1984) as well providing habitat for many aquatic species to fulfill various life stages, such as spawning (Kondolf & Wolman, 1993) or egg incubation (Greig et al., 2005). Measuring and mapping grain size has long been recognized as important to understanding where species can successfully fulfill various components of their life cycle, but manually measuring grain size over large spatial scales is extremely time consuming (Warrick et al., 2009) and the usefulness of automated tools to map sediments has long been recognized (Butler et al., 2001). Historically, a common approach to representing grain size in hydraulic and ecological models was to identify and measure one or more cross sections which were deemed broadly characteristic of a study reach (e.g., Bovee, 1982). However, this approach has many limitations, as most streams do not exhibit homogeneous Grain size distributions (GSDs), even across short reaches. Further, with the advancement of bathymetric data collection and multi-dimensional hydraulic modeling, there is a misalignment between available resolution of key habitat metrics, such as water depth and velocity, with grain size information of equivalent scale and resolution.

Writing – review & editing: James S. White, Karen Bartelt, Brandon T. Overstreet

As new methods to collect high resolution imagery and topography have advanced, novel techniques have been developed to increase both the spatial range and resolution of grain size data. This work expands on these previous efforts and brings them to a challenging environment and scale—grains beneath the water surface across over 260 km of geomorphically diverse river corridors in the Santiam River Basin, Oregon.

Many studies have investigated non-contact methods to map grain size at various resolutions, with approaches generally falling into three categories: (a) Measuring or extracting grain size from ground-based or aerial digital imagery, which can be further divided into two fundamentally different techniques that Buscombe et al. (2010) termed "geometrical," whereby individual grains are manually or automatically segmented and measured (e.g., Detert & Weitbrecht, 2012; Graham et al., 2005; Purinton & Bookhagen, 2019; Sime & Ferguson, 2003) and "statistical," which itself has several submethods (Buscombe, 2013; Buscombe et al., 2010; Buscombe & Masselink, 2009; Carbonneau et al., 2004; Rubin, 2004; Warrick et al., 2009); (b) using the signal return intensity or backscatter data from active sensors, such as sonar or lidar, and correlating these data with observed grain sizes (Bodine et al., 2024; Buscombe, 2017; Chardon et al., 2020); and (c) collecting high-resolution point clouds from a variety of instruments and methods, such as sonar, lidar, and photogrammetry, from which the vertical variation in point elevations is correlated to observed grain size (Brasington et al., 2012; Carrivick & Smith, 2019; Chardon et al., 2020; Detert et al., 2018; Groom et al., 2018; Heritage & Milan, 2009; Neverman et al., 2019; Storz-Peretz & Laronne, 2013; Vázquez-Tarrío et al., 2017; Woodget & Austrums, 2017). Machine learning approaches have also been developed which seek to combine disparate data sets to inform grain size mapping (Díaz Gómez et al., 2022).

Each approach and instrument used in these studies has its own suitable applications and limitations, with varying ability for measuring submerged grain size. Digital image processing can provide impressive resolution and accuracy but such approaches can be affected by shadows, available light, grain imbrication and shape, and viewing geometry. Both geometrical and statistical image processing applications have typically focused on above-water conditions, though Carbonneau et al. (2005) used aerial imagery to quantify submerged grain size in shallow areas along 80 km of river. Some studies have suggested it might be feasible to use underwater photos to measure submerged grain size, though results are sensitive to biofilm and lack of light and are limited in their ability to capture large swaths of submerged sediment (Chardon et al., 2020). Correlating the return intensity or backscatter data of Lidar and sonar sensors with grain size has shown promising results, and studies have used a variety of instruments, including recreational side scan sonar (Bodine et al., 2024; Buscombe, 2017), survey grade multibeam sonar (Lamarche et al., 2011), and near-infrared (NIR) Lidar (Chardon et al., 2020). Recreational sonars are inexpensive and might be able to produce reliable submerged grain-size information at relatively large scales, but current analysis of this data is limited to broad categorization of grain size, such as fines, hard substrates, and boulders, rather than specific quantification of sizes (Buscombe, 2017; Bodine et el., 2024). Further, this approach requires operating a vessel throughout the reach of interest, which can be time-consuming and potentially infeasible due to shallow water or unsafe water conditions. Survey grade multi-beam sonar has been shown to produce estimates of grain size (Lamarche et al., 2011), but instruments can be cost-prohibitive and are limited in shallow rivers, where water depth limits sonar swath-width. Airborne NIR Lidar can efficiently cover large areas and return intensities from Lidar have been shown to capture measured grain size reasonably well (Chardon et al., 2020), but these are limited to exposed bars and thus miss important area beneath the water surface. Sonar, NIR Lidar, and photogrammetry have been used to generate high-resolution point clouds from which the vertical variation of elevations, or roughness, can be calculated and correlated with measured grain size (Chardon et al., 2020; Hiller et al., 2023; Vázquez-Tarrío et al., 2017). This approach may provide many advantages, however, no known study has investigated the viability of bathymetric ("green") Lidar at the site, reach, or river scale for measuring grain size.

Typical terrestrial Lidar emits photons in a near-infrared (NIR) band (wavelength $\{\lambda\} = 1{,}064$ nm) of the electromagnetic spectrum to map surfaces and features. However, radiation of this wavelength is rapidly attenuated by water molecules and thus NIR lidar is limited to mapping features above the water surface. In contrast, bathymetric lidar emits photons in a green wavelength ($\lambda = 532$ nm), which is better able to travel through the water column and reflect off the bed surface. Thus, bathymetric Lidar could offer a plausible approach to mapping grain sizes throughout a river. The potential utility of bathymetric Lidar to characterize riverine habitats has been recognized since at least the 1990s (Kinzel et al., 2007; Tiffan et al., 2002), and significant work has occurred since then to develop methods to collect, process, and analyze Lidar data to inform aquatic habitat quality and quantity (Duffin et al., 2021, 2023; McKean et al., 2008, 2009). This study investigates the feasibility of using

large-scale, commercially available bathymetric Lidar data to evaluate its potential for mapping submerged grain size across a large spatial extent (260 km). Results from this analysis are then compared to field measurements and contextualized by relating modeled grain size to suitable sediment size for spawning Chinook salmon to determine available habitat across geomorphically diverse rivers and nearly the full extent of observed spawning in the Santiam River Basin, Oregon.

1.1. Study Area

The Santiam River Basin in northwestern Oregon drains 4,660 km^2 of the Cascade Range (Figure 1). The watershed originates on the western flanks of Mount Jefferson (~3,200 m elevation) and flows westward to its confluence with the Willamette River (49 m elevation). Upper reaches consist of younger, highly permeable High Cascades volcanics and volcaniclastics, with older Western Cascades volcanics in the middle reaches, and the lower reaches within the alluvial plain of the Willamette Valley (Tague & Grant, 2004). Rivers throughout the study area are generally gravel- or cobble-bedded and exhibit a variety of channel planforms, though plane-bed is the dominant morphology. There are four high-head multi-purpose dams in the basin and study area that are primarily operated for flood control: two on the North Santiam River and two in the South Santiam River Basin. In addition to impounding water, these dams capture an estimated 94% and 91% of the total bed material flux in the North Santiam and South Santiam Rivers, respectively (O'Connor et al., 2014). Low-flow wetted channel width varies substantially throughout the study area, with the uppermost reaches generally spanning 10–15 m wide, whereas reaches downstream of dams typically span 30–60 m, as measured from aerial imagery and Lidar (Table 1).

The Santiam River Basin provides critical spawning and rearing habitat for Chinook salmon (*Oncorhynchus tshawytscha*), which are listed as threatened under the Endangered Species Act (NOAA, 2021). These fish need specific habitat types to fulfill various aspects of their lifecycle, including rearing, migration, holding, and spawning. Grain size is a critical component of the spawning life stage, where female salmon dig nests in streambed gravels in which they lay eggs. The eggs are then fertilized by males and subsequently covered with gravel to protect the nest (Kondolf & Wolman, 1993; McNeil & Ahnell, 1964). These clasts must be small enough that the fish can sufficiently move them to build their nests (Kondolf & Wolman, 1993; Riebe et al., 2014), yet large enough to resist movement and adverse scour of buried eggs during common flows (Montgomery et al., 1996). Identifying where and how much sediment falls within this suitable range of grain sizes for spawning is often an important concern to river managers and stakeholders. Such data may help inform a variety of management decisions such as streamflow management and dam releases during spawning seasons, river restoration and gravel augmentation, or assessments of habitat availability in reaches proposed for re-introduction of species that have been extirpated.

2. Methods

Topo-bathymetric Lidar data (henceforth Lidar data) was collected using a Riegl 880G (green) and a Riegl 880GII (near infrared) instrument between 23 August 2023, and 4 September 2023 (NV5 Geospatial, 2023), which coincides with annual low flows within the Santiam River. Underwater point locations were corrected for refraction by applying Snell's Law to a water surface elevation model (NV5 Geospatial, 2023). The Lidar data was collected on a crewed, fixed-wing aircraft from 400 to 1,100 m above ground level at a speed of 130–145 knots, with a 60%–70% swath overlap. The average density of bathymetric points was 10.4 points/m^2, although there is significant spatial variation throughout the study area, ranging from 0 points/m^2 to over 30 points/m^2. Lidar collection specifications were consistent with typical U.S. Geological Survey (USGS) 3D Elevation Program (3DEP) Quality Level 1 (QL1) and Quality Level 2 (QL2) specification (The Interagency Working Group on Ocean and Coastal Mapping, 2018), which is to say that no unique specifications (e.g., higher swath overlap, lower flight altitude, etc.) were added to perform this study.

Accuracy of the Lidar data was evaluated by comparing Lidar points to locations surveyed with high precision Global Navigation Satellite System (GNSS) equipment and details of this effort can be found in the associated report (NV5 Geospatial, 2023). Ground control points were collected in locations having a variety of landcover, including vegetated and submerged locations. Lidar alignment with ground surveys varied between land cover, with root mean square error (RMSE) values as low as 0.03 m in non-vegetated exposed surfaces, to 0.053 m for bathymetric points. Horizontal accuracies varied by flight height, with flights at 500 m above ground level having

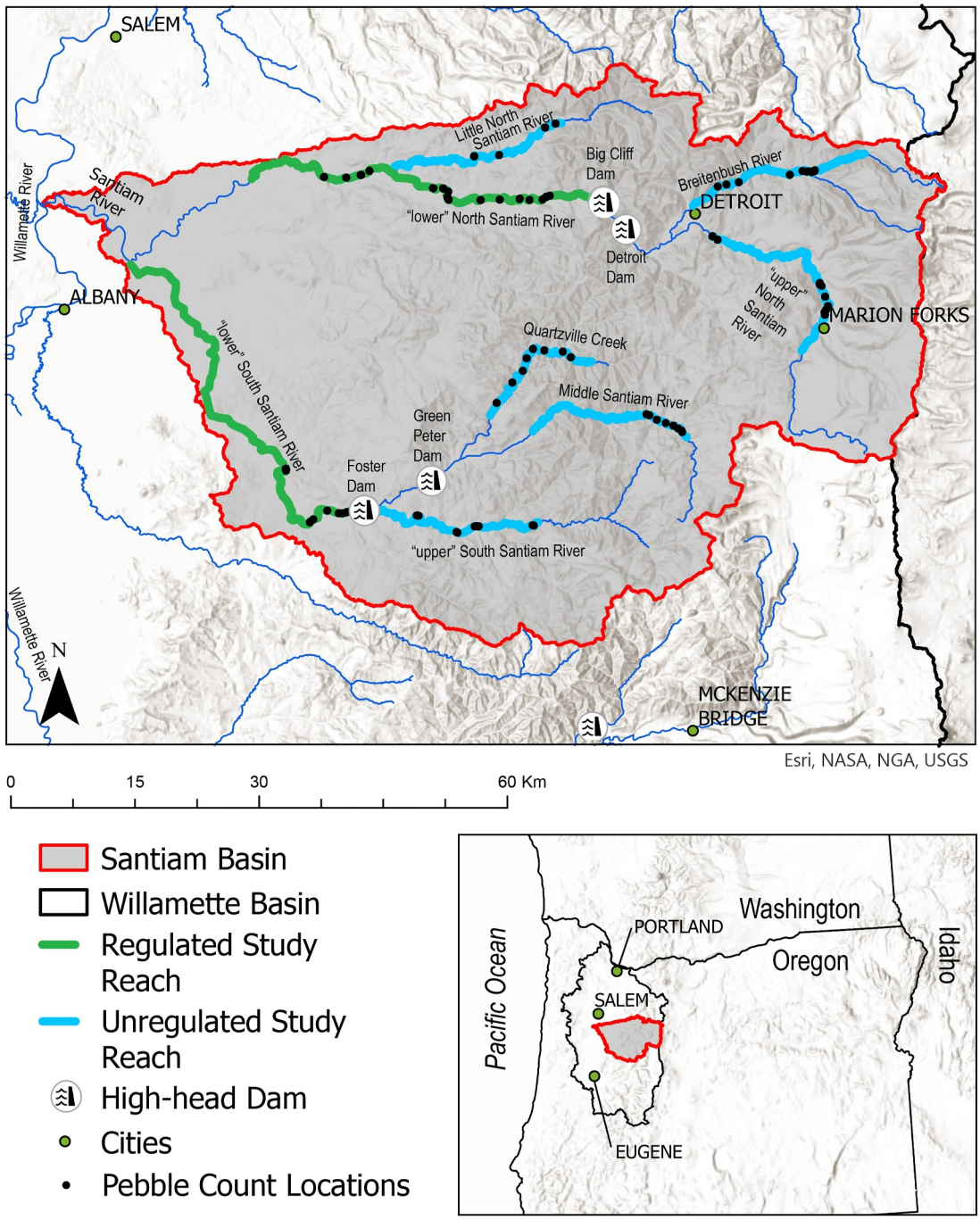

Figure 1. Map of the Santiam River Basin (red polygon). Thick blue and green lines indicate the extent of study reaches, while small black points indicate locations of pebble counts.

horizontal RMSE values of 0.081 m while flights at 1,100 m above ground level having horizontal RMSE values of 0.173 m. Precision of the Lidar data was not evaluated during data collection, but manufacturer specifications report 0.025 m precision (NV5 Geospatial, 2023).

The Lidar data coverage spans the approximate extent of Chinook salmon spawning within the Santiam River Basin and includes eight reaches spanning five rivers. The study reaches include: The North Santiam River below Big Cliff Dam (named "lower North Santiam" for this study), Little North Santiam River, Breitenbush River, North Santiam River above Detroit Reservoir (named "upper North Santiam" for this study), the South Santiam

Table 1
Reach Characteristics and Summaries of Lidar Point Density and Pebble Count Metrics, Including the Means of the D_{50} (Median Grain Size) and D_{84} (Grain Size for Which 84% of the Particles Are Smaller Than) in Each River Basin

River	Average slope	Mean low-flow width (m)	Mean lidar point density (points per m^2)	Mean D_{50} (mm)	Mean D_{84} (mm)	Mean bed roughness (mm)	Number of pebble counts
Breitenbush	1.44%	15.3	10.8	67	135	16	10
Little North Santiam	0.58%	22.4	9.4	54	103	16	5
lower North Santiam	0.43%	60.3	17.2	61	118	14	20
lower South Santiam	0.16%	55.2	17.7	64	117	13	11
Middle Santiam	1.20%	17.2	13.1	91	165	25	10
Quartzville	1.11%	15.4	9.4	55	102	19	11
upper North Santiam	1.12%	22.5	9.8	102	195	20	10
upper South Santiam	0.67%	20.8	9.2	59	104	16	10

Note. Shaded rivers are unregulated (upstream of dams), while unshaded reaches are immediately downstream of dams.

River below Foster Dam (named "lower South Santiam" for this study), Quartzville Creek, the Middle Santiam River, and the South Santiam River above Foster Reservoir (named "upper South Santiam" for this study) (Figure 1). Point cloud and rasterized Lidar data are available on The National Map (U.S. Geological Survey, 2024).

Grain size data were collected using Wolman (1954) pebble counts, where field crews identified shallow areas (generally less than 1 m deep) with relatively consistent distributions of surficial grain size, similar to methods described in Buffington and Montgomery (1999a). Sampling areas were established by visually identifying facies breaks between dominant grain sizes and then randomly selecting and measuring the intermediate (b) axis of at least 100 grains using a gravelometer along transects roughly perpendicular to the shore (Figure 2). Grains smaller than 2 mm were binned as 2 mm, while the b-axis of grains larger than 256 mm were estimated. For facies units that were not large enough for perpendicular transects, additional transects were collected parallel to shore until at least 100 clasts were measured. At least 10 pebble counts were collected on all rivers in this study, except the Little North Santiam River, where limited access restricted the number of pebble counts to five (Figure 1). Sites were selected such that there was a large range of median grain sizes measured within each sub-basin. For example, fine-, moderate-, and coarse-grained bars were intentionally targeted within each reach to bound commonly observed sediment sizes (Figure 3). GSDs and summary metrics, including the median grain size (D50) and sizes for which 16% and 84% of the sediment are smaller (D16 and D84, respectively) were calculated at each measurement site. The location of each grain size measurement was collected with GNSS equipment using real time kinematic, network, or post-processed corrections. The horizontal precision of these points varied but was generally less than 0.05 m. Finally, using the "simple features" package in R (Pebesma, 2018), a polygon was generated around these points representing the boundary of each submerged measurement location (Figure 2). The area of these sites ranged from 7 to 450 m^2 with a median of 60 m^2. Sampling locations were distributed throughout each river to the extent possible, but limited site access prevented even distribution of measurements in certain rivers.

Surface roughness of the streambed (henceforth roughness) is the vertical variation between the elevation of a point and the elevation of surrounding points. There are several ways roughness can be calculated, but methods generally compare each point to surrounding points within a specified area and use various summary metrics to define the vertical variation within the area. Summary metrics defining roughness include doubling the standard deviation of local elevations, detrending the local surface and taking the standard deviation of heights, or the vertical difference in height between a point and a planar surface of surrounding points. Vázquez-Tarrío et al. (2017) compared three roughness metrics to measured grain size data and found that the roughness height, or the difference in height between a point and a surrounding locally averaged horizontal plane, was the most

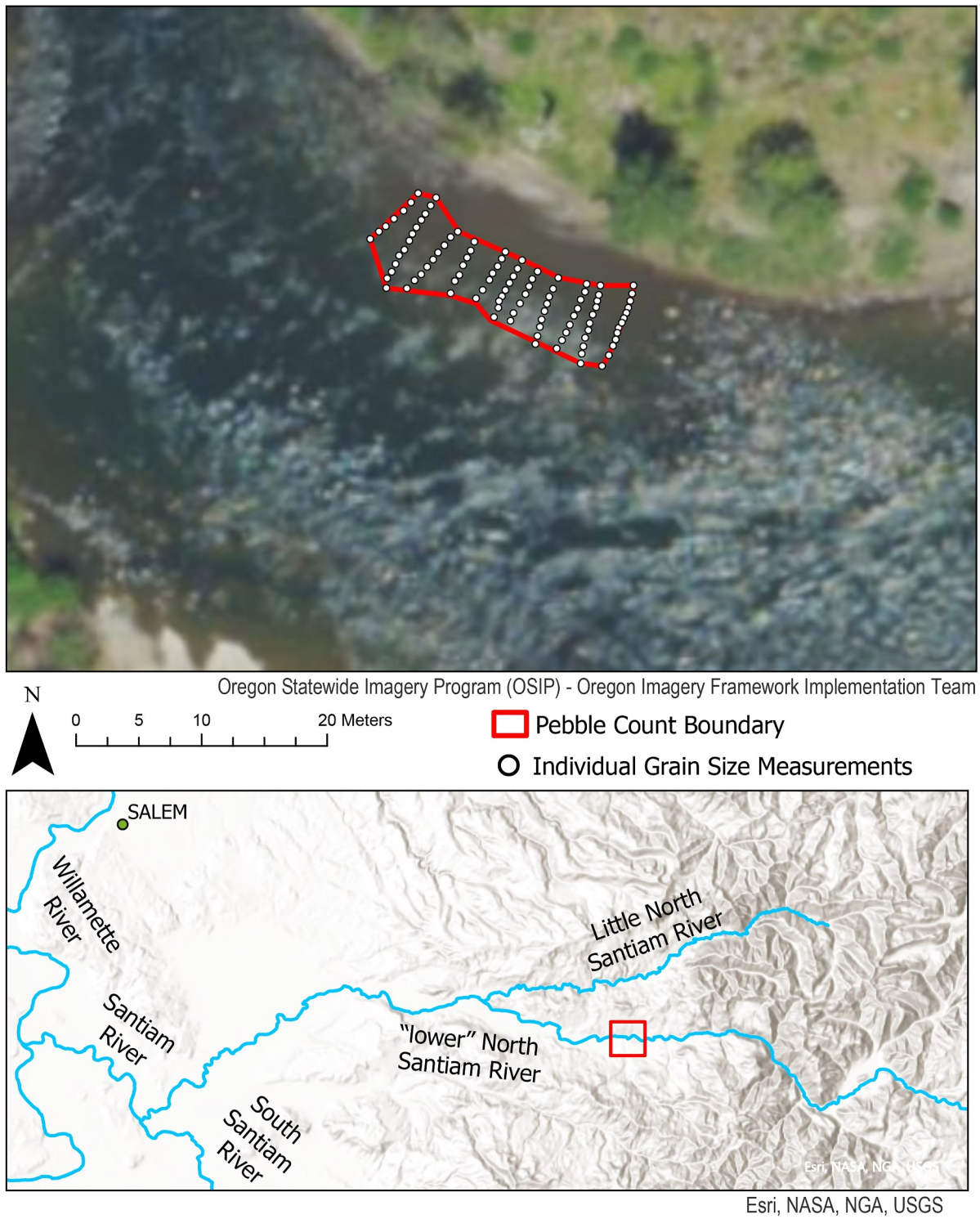

Figure 2. Example of georeferenced pebble count collected on the North Santiam River.

accurate surrogate for grain size. For each lidar tile (a 1 km^2 subset of the larger data set), this roughness height metric was calculated for each bathymetric point using a 1 m kernel radius using the open-source CloudCompare software (CloudCompare, 2.13.1, 2022) run through the R programming platform (R Core Team, 2024). Roughness point clouds were then rasterized at a 1 m^2 resolution using the lidR package in R (Roussel

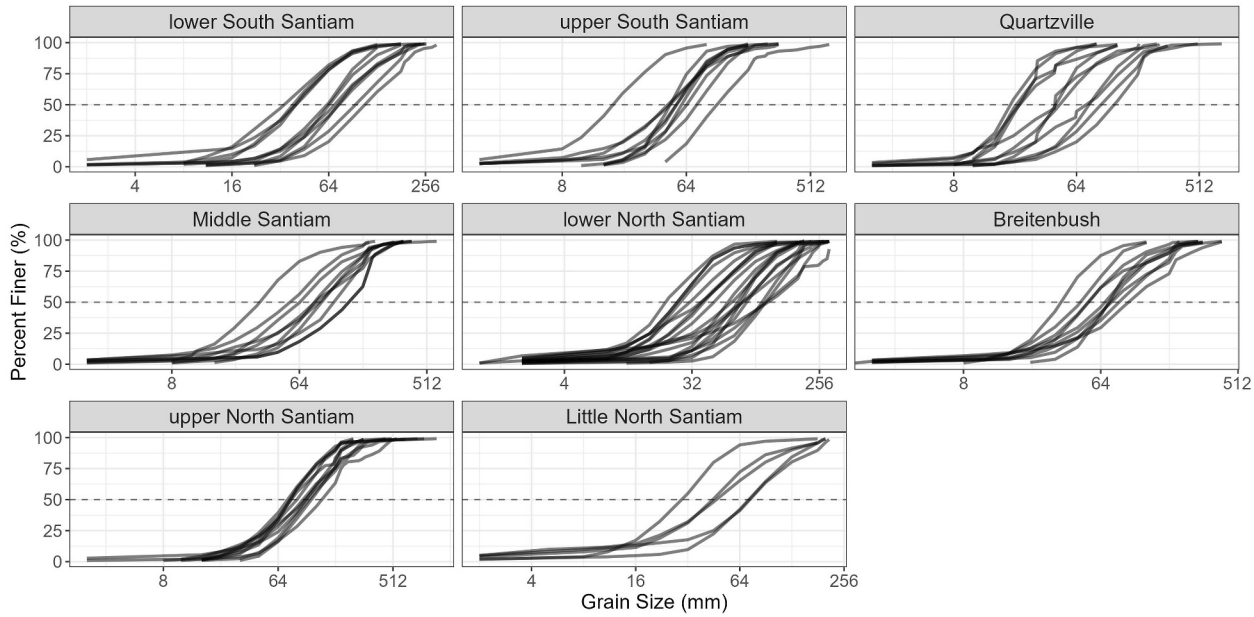

Figure 3. Grain size distributions from individual pebble counts within each river sub-basin of the study. Note that *x*-axis scaling differs between panels.

et al., 2020). The 1 m kernel radius was selected as it is about three times the size of the largest b-axis measured in most pebble counts. This ratio was advised by Chardon et al. (2020), who found that correlation of roughness and measured grain size was relatively consistent with kernel radius values of less than 1.4 m, above which correlations became weaker. Once roughness raster were generated for the Lidar tiles, they were merged into a single raster for each river and Lidar-derived roughness metrics were extracted within pebble-count polygons. Roughness summary metrics were then compared to measured grain size data in each pebble count polygon.

Results from Vázquez-Tarrío et al. (2017) suggest two important criteria for correlating measured grain size with roughness. One is a minimum Lidar point density of 5–6 points/m^2 to establish a relation between roughness and grain size, with marked improvements with increasing point density to about 11 points/m^2, above which minimal additional accuracy is gained. While the mean point density of the bathymetric returns is 10.4 points/m^2, there are areas with lower point density, primarily due to deepwater (>3 m) and/or vegetation overhanging the river channel. As a result, a 1 m^2 point-density raster was generated across the study extent and areas where point densities were less than 5 points/m^2 were removed from analysis. A second criterion identified by Vázquez-Tarrío et al. (2017) was the need for eight or more samples for generating a stable slope coefficient in roughness-grain size relations. All but one river reaches of this study had a minimum of nine pebble counts (Table 1); only five samples were collected on Little North Santiam due to limited access.

Regression analyses were performed to correlate measured grain sizes with Lidar roughness at both the individual river reach and full study area extent. Median, mean, 84th, and 16th percentile roughness values in each polygon were extracted and compared to D_{16}, D_{50}, and D_{84} metrics from the associated pebble count data. River-specific regression models were then applied to the roughness height raster to create raster of modeled grain sizes. In addition to river-specific regression models, a single regression using data collected across all rivers was generated and applied to each river to assess the need and value of generating river-specific regressions compared to a single regression for the entire basin. Two iterations of the regression using all data were developed–one with no weighting and one where each measurement was weighted by the total number of measurements within the reach divided by reach length.

Model performance was assessed by goodness-of-fit statistics (including the coefficient of determination {R2}, root mean square error {RMSE}, and percent bias {PBIAS}) for measured grain-size percentiles (D16, D50, D84) versus mean lidar roughness in each pebble-count polygon. GSDs were also predicted for each pebble-count location by summing 1 m^2 D_{50} predictions across the pebble-count polygon and visually compared to observed GSDs. Note that the predicted GSDs are distributions of modeled D_{50} values, which are

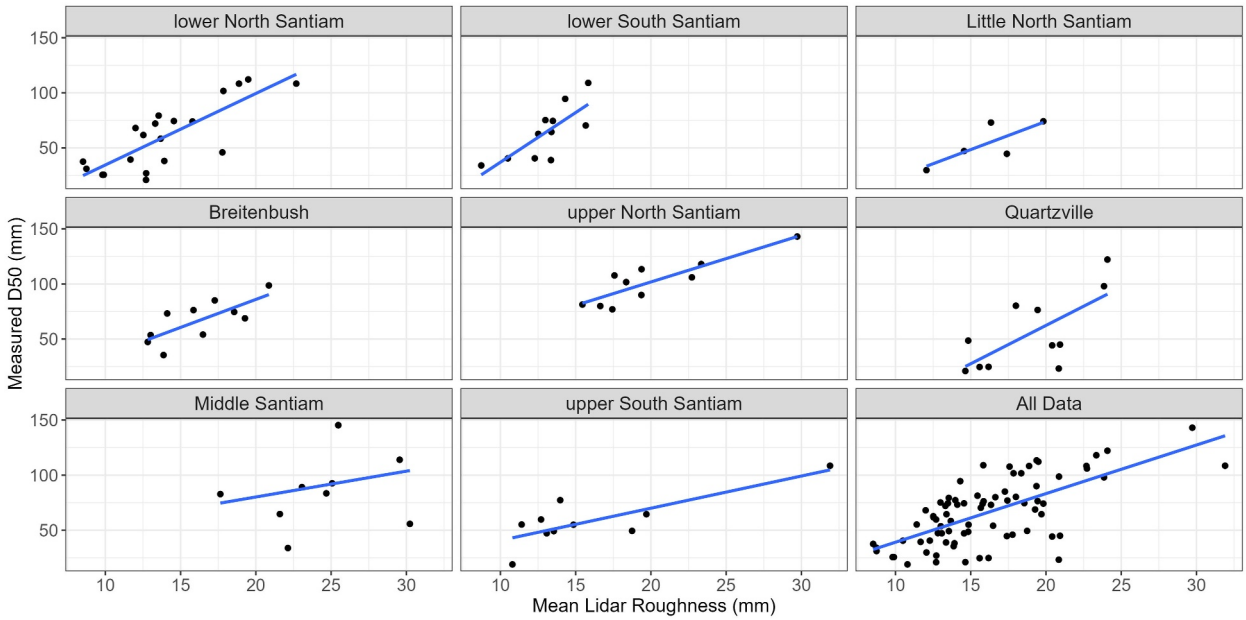

Figure 4. Measured D_{50} (median grain size) from each pebble count compared to mean Lidar roughness for each river and all reaches combined (lower right plot).

methodologically different from Wolman pebble counts that randomly sample all sizes within the pebble-count polygon. In the above analyses, grain size was capped at 300 mm due to limited observation of coarser sizes.

Suitable grain size is one of several important habitat components influencing where Chinook salmon spawn. As an example of how the present approach could be applied to this issue, modeled grain sizes were classified to assess the availability of suitable sediment sizes for spawning Chinook salmon. Several methods have been developed to relate grain size to spawning habitat for Pacific salmon (*Oncorhynchus spp.*). For example, Riebe et al. (2014) developed an approach to evaluate the fraction of the bed that can be mobilized by a fish of a given length, using the ratio of the D_{50} and D_{84} grain sizes; however, no known spawning fish-length data have been collected in the Santiam River Basin to facilitate such analysis. For this study, a literature review was conducted to assess the range of grain sizes suitable for spawning Chinook salmon in the Pacific Northwest, USA. From this analysis, a D_{50} range of 17–59 mm was determined (Supporting Information S1). This grain size range is adopted here to demonstrate the application of the method; additional research could help to identify population-specific sediment requirements in the Santiam River Basin. Other important physical metrics such as water depth, velocity, temperature, and hyporheic exchange are not considered in this analysis, nor are biological factors, such as proximity to natal spawning grounds.

To evaluate the accuracy of predicted spawning habitat, model results were compared to redd locations that were surveyed along five of the study reaches in fall, 2024. These were opportunistic surveys, where active spawning was observed over the course of 2 weeks when spawning activity is typically high. Redd locations were documented using GNSS equipment using real time and post processed corrections, resulting in horizontal precisions generally under 0.1 m. These locations were then compared to predicted D_{50} values classified by spawning suitability to evaluate model accuracy. The data presented here are not an exhaustive compilation of where salmon spawned throughout these reaches; rather the data help to contextualize the spawning suitability results of this study.

3. Results

Results comparing measured D_{50} and D_{84} grain size to mean Lidar roughness using a linear regression suggest a strong but varying relationship between rivers. For the D_{50} linear regression, the coefficient of determination (R^2) ranged from 0.47 to 0.76 across the study reaches, with a mean of 0.61 (Figure 4, Table 2). RMSE values ranged from 9.51 to 23.56 mm, with a mean of 14.50 mm, while percent bias (PBIAS) values ranged from 1.0% to 22.1%, with a mean of 8.6% (Table 2). The unweighted study-wide regression resulted in an R^2 of 0.45, RMSE of

Table 2
Regression Details, Results, and Goodness of Fit Statistics for D_{50} (Median Grain Size) and D_{84} (84th Percentile Grain Size) Regressions

	D50 Model					D84 Model				
River	Intercept	Slope	R2	RMSE (mm)	PBIAS	Intercept	Slope	R2	RMSE (mm)	PBIAS
Breitenbush	−15.62	5.08	0.55	12.02	4%	−58.07	11.88	0.54	29.07	−7%
Little North Santiam	−28.41	5.13	0.61	10.83	4%	−65.86	10.55	0.67	19.25	−5%
lower North Santiam	−30.34	6.49	0.65	17.58	13%	−79.76	14.15	0.72	32.66	−11%
lower South Santiam	−53.14	9.01	0.59	14.75	5%	−90.09	15.90	0.60	25.37	−5%
Middle Santiam	33.3	2.34	0.06	33.28	18%	126.38	1.57	0.02	42.21	−11%
Quartzville	−76.73	6.96	0.48	23.57	22%	−133.00	12.40	0.49	41.19	−21%
upper North Santiam	17.02	4.24	0.76	9.52	1%	−1.03	9.78	0.70	25.46	−2%
upper South Santiam	11.57	2.92	0.63	13.27	10%	21.43	5.11	0.64	22.58	−8%
All Data	−5.01	4.41	0.45	21.5	17%	−16.50	8.82	0.46	42.34	−17%

Note. Shaded reaches are unregulated (upstream of dams), while unshaded reaches are subject to flow regulation (downstream of dams). RMSE, root mean square error (mm); PBIAS, percent bias.

21.50 mm and a PBIAS of 16.8%, while the regression weighted by pebble counts per kilometer was nearly identical. The regression slope coefficients between reaches range from 2.3 to 9.0, while *Y*-intercept values ranged from −76.73 to 17.02 mm. Results from the D_{84} regression to the mean Lidar roughness value show generally similar goodness of fit statistics compared to the D_{50} regression (Table 2). Correlations between Lidar roughness and measured D_{16} values showed statistically significant but weak relations and therefore are not included. Correlations between measured D_{84} and 84th percentile roughness showed similar though slightly weaker correlations, compared to the D_{84} to mean roughness regression.

The Middle Santiam River had unresolved GNSS issues, resulting in partially corrected solutions, which were visibly not aligned with co-collected Ortho-imagery. Consequently, the resulting pebble count polygons do not align precisely with the Lidar data, which resulted in little to no trend between grain-size and Lidar roughness (Figures 4 and 5, Table 2).

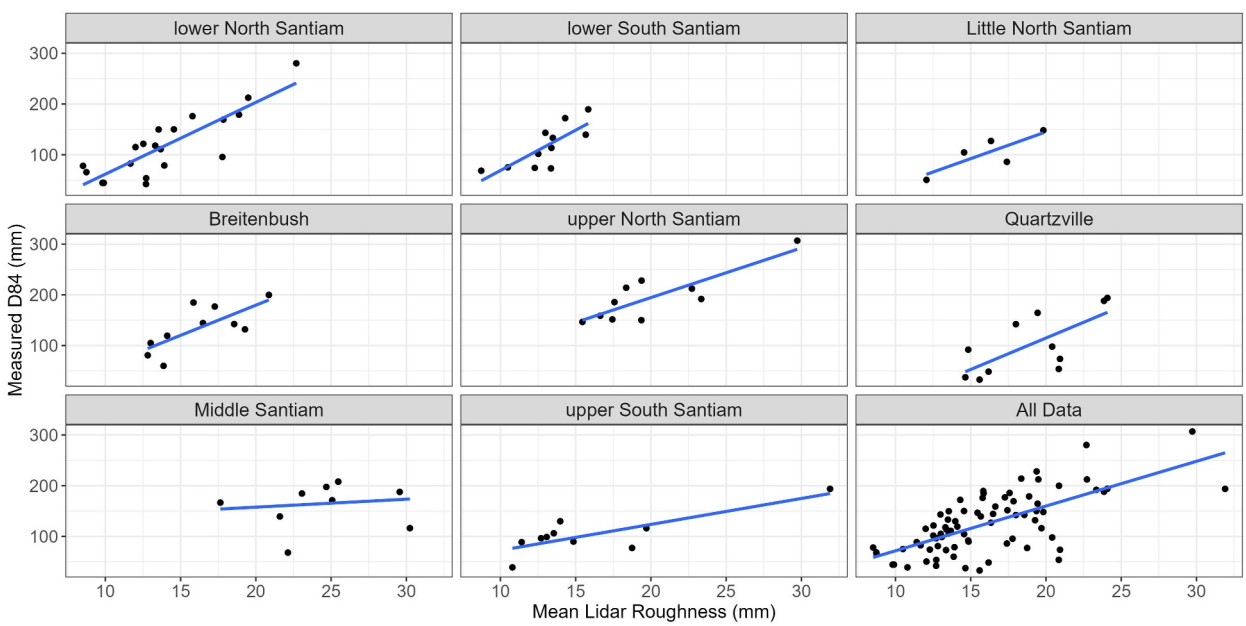

Figure 5. Measured D_{84} (84th percentile grain size) from each pebble count compared to mean Lidar roughness for each river and all reaches combined (lower right plot).

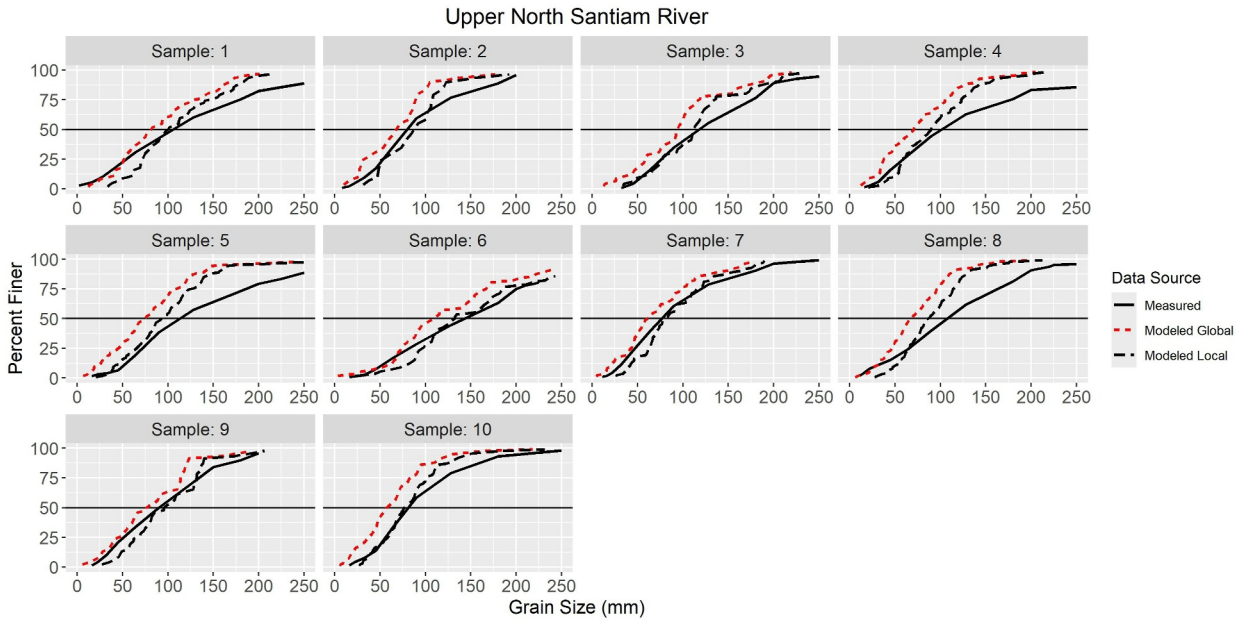

Figure 6. Modeled versus measured grain size distributions at sampled locations on the unregulated upper North Santiam River. Horizontal black line represents the D_{50} (median grain size) of the sample/model.

Measured and modeled GSDs were visually compared to assess the model's ability to replicate the full distribution of observed grain sizes within a measured polygon. As a result, the watershed-wide regression of grain size data was applied to the Middle Santiam River Lidar data, and these model results were compared to measured GSDs. Results show reasonably good agreement (Figures 6 and 7 show examples for the upper and lower North Santiam River, additional reaches found in the Supporting Information S1). Given the errors discussed above for the Middle Santiam River, the watershed-wide regression of grain size was used to determine modeled GSDs in that reach. The larger rivers downstream of high-head dams generally have the strongest agreement between measured GSDs and those derived from the 1 m^2 grain size model, which is likely attributable to the higher point densities in

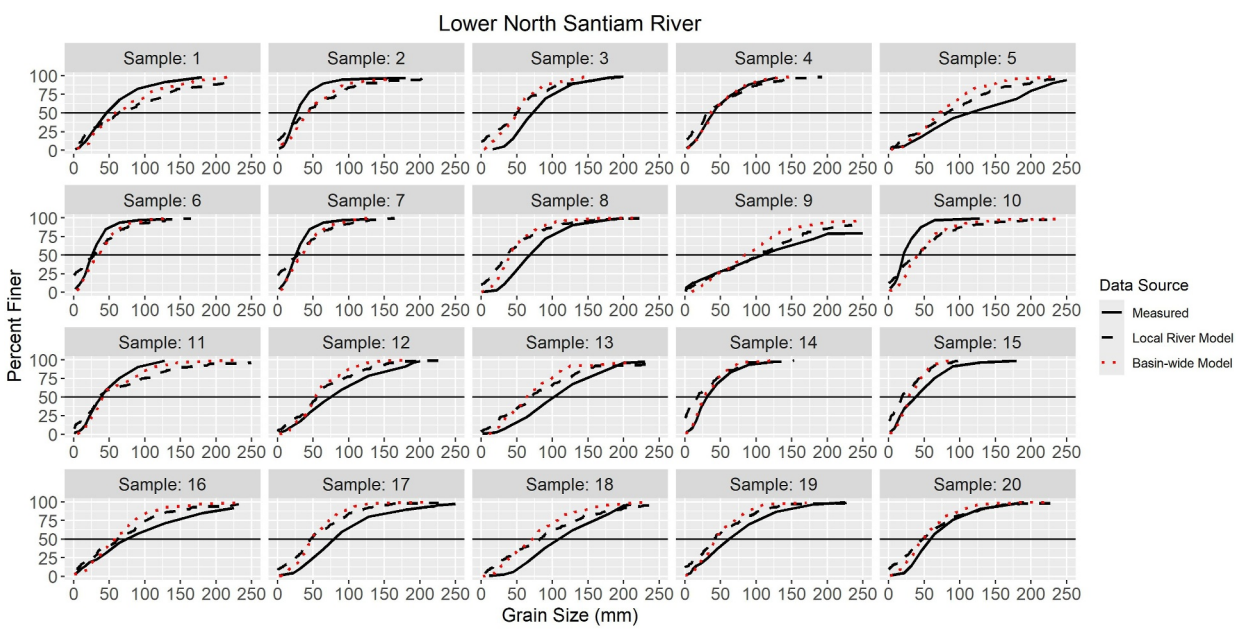

Figure 7. Modeled versus measured grain size distributions at sampled locations on the regulated lower North Santiam River. Horizontal black line represents the D_{50} (median grain size) of the sample/model.

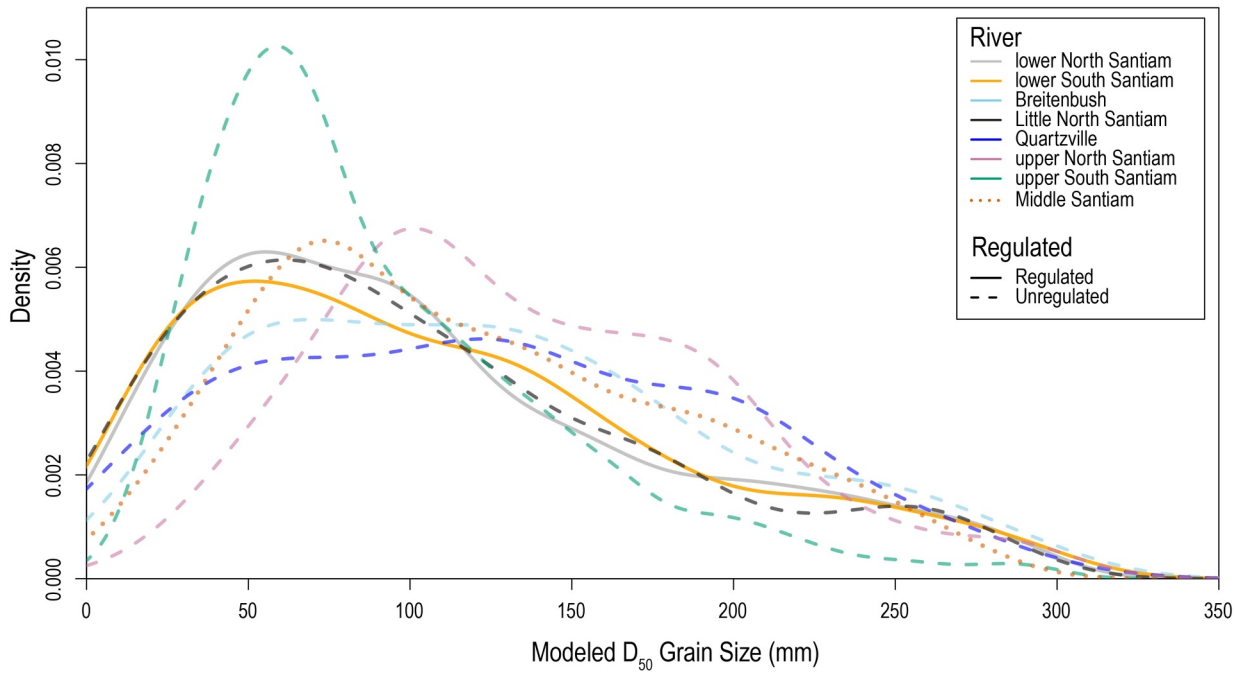

Figure 8. Probability density distribution of modeled D_{50} (median grain size) throughout each river and the entire study area (dashed black line). All results use the river-specific D_{50} grain size model (Figure 4), except the Middle Santiam River.

these reaches. The rivers upstream of dams capture general trends reasonably well, yet some of these upstream reaches show a bias toward over estimating grain size, which may be attributable to lower point densities in these reaches. GSDs determined from the basin-wide model are similar to the river-specific although the latter more closely aligns with measured GSDs.

Once grain size maps were generated, the distribution of modeled D_{50} throughout each river was compared (Figure 8) to assess basin-wide patterns in GSD. Results from this analysis highlight the diversity of GSDs across the basin, where the upper South Santiam River has a notably finer distribution than the other sites, while the upper North Santiam River and Quartzville Creek reaches have slightly higher abundance of large cobble (specifically spanning about 150–225 mm) compared to the other sites. There are no consistent differences in GSD between the regulated and unregulated rivers analyzed.

Comparing geolocated Chinook salmon redds to modeled grain size suitability shows that in four of the five reaches containing redds, more than 70% of redds were observed at locations classified as having "suitable" (Figure 9) grain sizes for Chinook salmon spawning. The most common erroneous classification was where redds were observed at locations classified as "too coarse", while two reaches had 3%–10% of redds observed in areas classified as "too fine." The notable exception in these results is from the upper North Santiam, where over half (54%) of redds were observed in locations classified as "too coarse," with the remainder (46%) classified as "suitable."

Predictions for the entire study area further show that patterns of usable spawning sediment are highly variable between the regulated and unregulated rivers. In the larger regulated reaches, spawning habitat is generally more organized and clustered into larger areas that are often surrounded by finer sediments (Figure 10). In contrast, in most of the unregulated reaches, suitable spawning sediment is disorganized and consists largely of small patches throughout each river (Figure 11). The notable exception to this is the upper South Santiam River, which contains extensive areas of suitable spawning. Comparing the amount of suitable spawning material relative to the total bed area within each river reveals a spectrum of suitability throughout the watershed. The upper South Santiam has the largest amount of suitable spawning sediment relative to the area in that river available for analysis (where Lidar point densities were greater than 5 points/m^2), with 31% of the area within suitable sediment ranges. This site is anomalous compared to the other unregulated study reaches, which range between 7% and 20%. The regulated study reaches, the lower North and lower South Santiam, have similar amounts of relative available

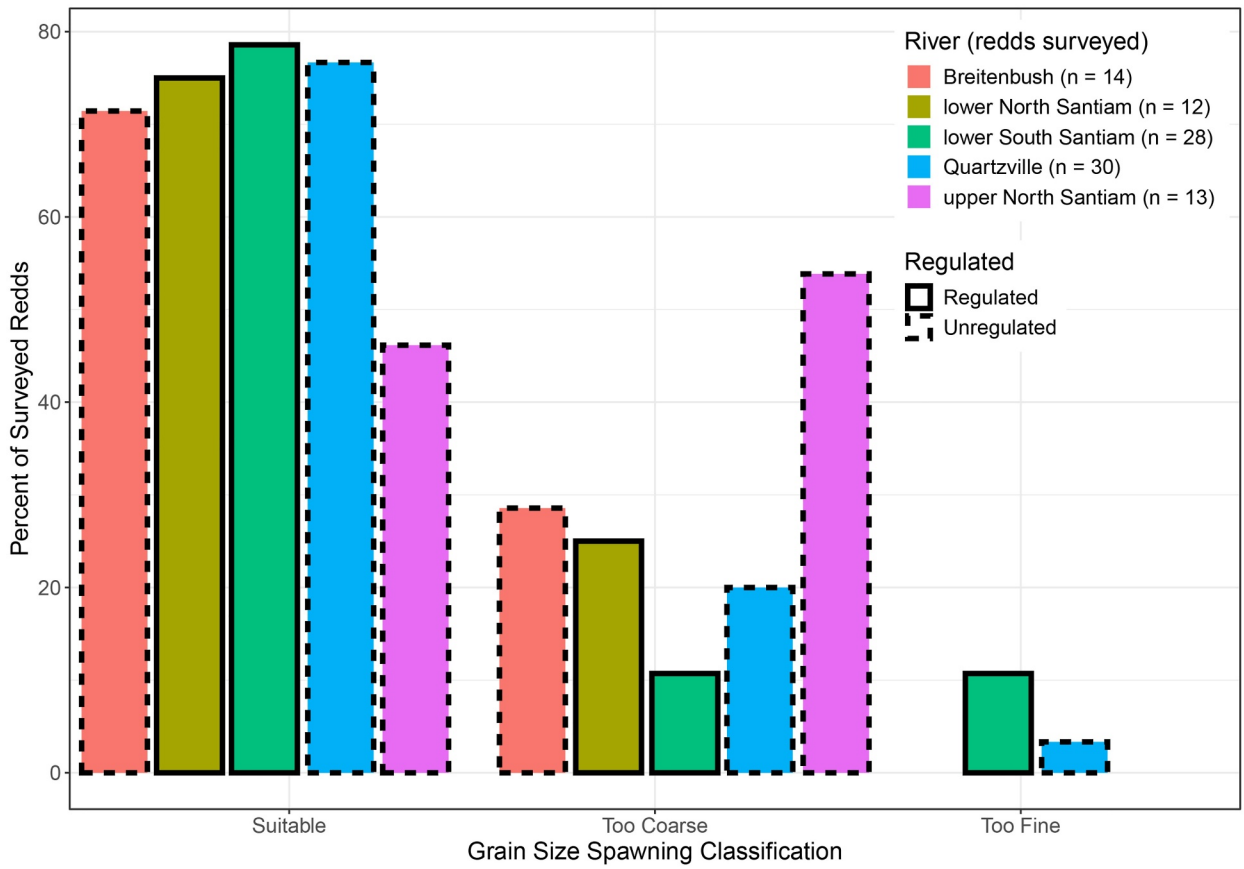

Figure 9. Comparison of observed Chinook salmon redd locations with modeled grain size classified by spawning suitability. Bars with solid outlines indicate reaches regulated by upstream high-head dams, while bars with dashed outlines indicate unregulated reaches.

spawning sediment; representing 21% and 18% of their respective areas available for analysis. The lower North Santiam River has by far the most absolute abundance of suitable spawning sediments, at 63.8 ha, which is a consequence of it being the longest and generally widest reach of river in this study. In contrast, the upper North Santiam River and Quartzville Creek have nearly the same amount of absolute suitable spawning sediments, with 3.5 and 3.3 ha, respectively.

4. Discussion

Results demonstrate that submerged bed-surface grain size can be characterized using commercially available airborne bathymetric Lidar across large spatial scales and geomorphically diverse river corridors, if point densities are sufficient. The statistical models developed quantified site-scale D_{50} and D_{84} metrics with a reasonable degree of accuracy and also generally matched full GSDs from sampled locations. The fact that modeled GSDs derived from summing predicted D_{50} values per square meter match measured GSDs at pebble count locations suggests that the 1 m^2 resolution is appropriate, however validation of results at this 1 m^2 scale are warranted. In particular, while the model predicts grain size at high resolution, results are tested at larger pebble-count scales (7–450 m^2). As such, prediction accuracy at smaller scales remains to be tested.

Two suites of statistical models were developed for this study: one was a regression model developed from data collected within each river, while the second was developed by combining data from all rivers, except for the Middle Santiam River, into a single regression. Findings suggest that although river-specific models out-perform basin-wide models, the differences are relatively small, even across significantly different channel morphologies. For example, there are no notable differences in models in smaller unregulated rivers compared to larger, downstream, regulated rivers. This comparison suggests that at the HUC-8 watershed scale (the size of the Santiam River Basin investigated in this study), a single relation between roughness and grain size may be

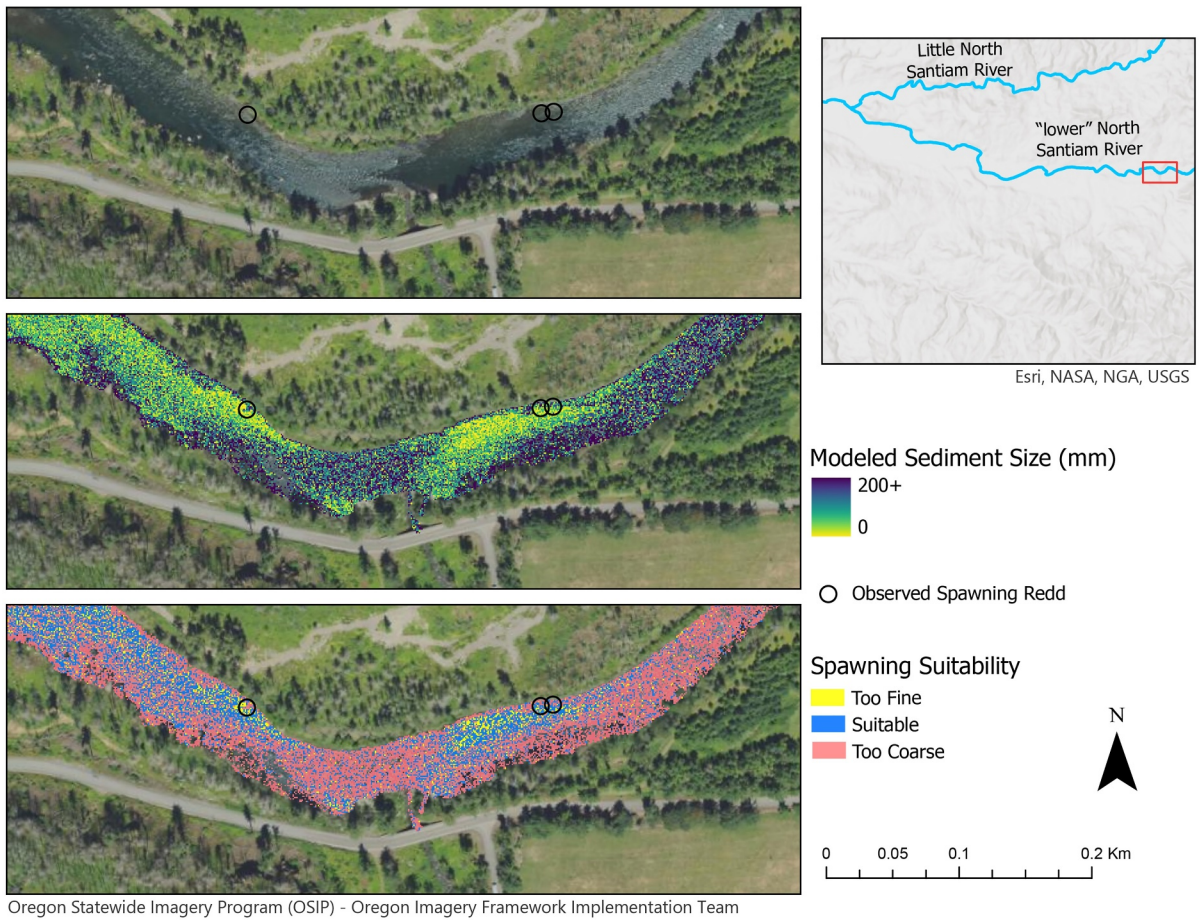

Figure 10. Modeled sediment size and spawning suitability on the regulated lower North Santiam River.

sufficient to characterize GSDs for applications where higher uncertainty is acceptable or if resources to collect field data are limited. More work would be needed to evaluate the spatial limits of broader scale roughness-grain size relationships, but such basin- or regional-wide relationships would reduce the amount of pebble count data needed in reaches where models are developed. Findings from the Middle Santiam River highlight this concept, as georeferencing errors prevented a river-specific relation in that portion of the stream network. Applying the watershed-wide relation to the Middle Santiam River resulted in similar GSDs to reaches with basin-specific data (Supporting Information S1), though the imprecise georeferencing of the Middle Santiam River data limits evaluation of model accuracy.

Although there was no statistically significant relationship between goodness-of-fit statistics to average Lidar point density, low point density resulted in relatively large areas removed from grain-size mapping in certain reaches. While individual patches of low point density are generally small, they combined to represent between 9% and 30% of each river in this study. The unregulated reaches have a greater relative area of sufficient point density coverage compared to the larger regulated reaches. The low point density areas in the smaller, unregulated reaches are not well organized and are generally scattered throughout the river corridor. In contrast, the low point density in the larger, regulated reaches are generally clustered in areas of deep water, where it was too deep for the Lidar to penetrate. This is attributable to the underlying cause of lower point density in each river type. In the smaller unregulated reaches, lower point density is a result of both vegetation and flight altitude. These smaller channels result in a greater proportion of the channel being covered by overhanging vegetation and the rougher terrain necessitated flying higher above ground compared to the downstream reaches. These findings are notable for future applications of this method; rivers with substantial overhanging vegetation will likely require lower flight elevation, stronger laser pulses, or multiple passes over the same location to achieve sufficient point densities, particularly if channel-wide coverage is important. Uncrewed aerial systems (UAS) or helicopters could

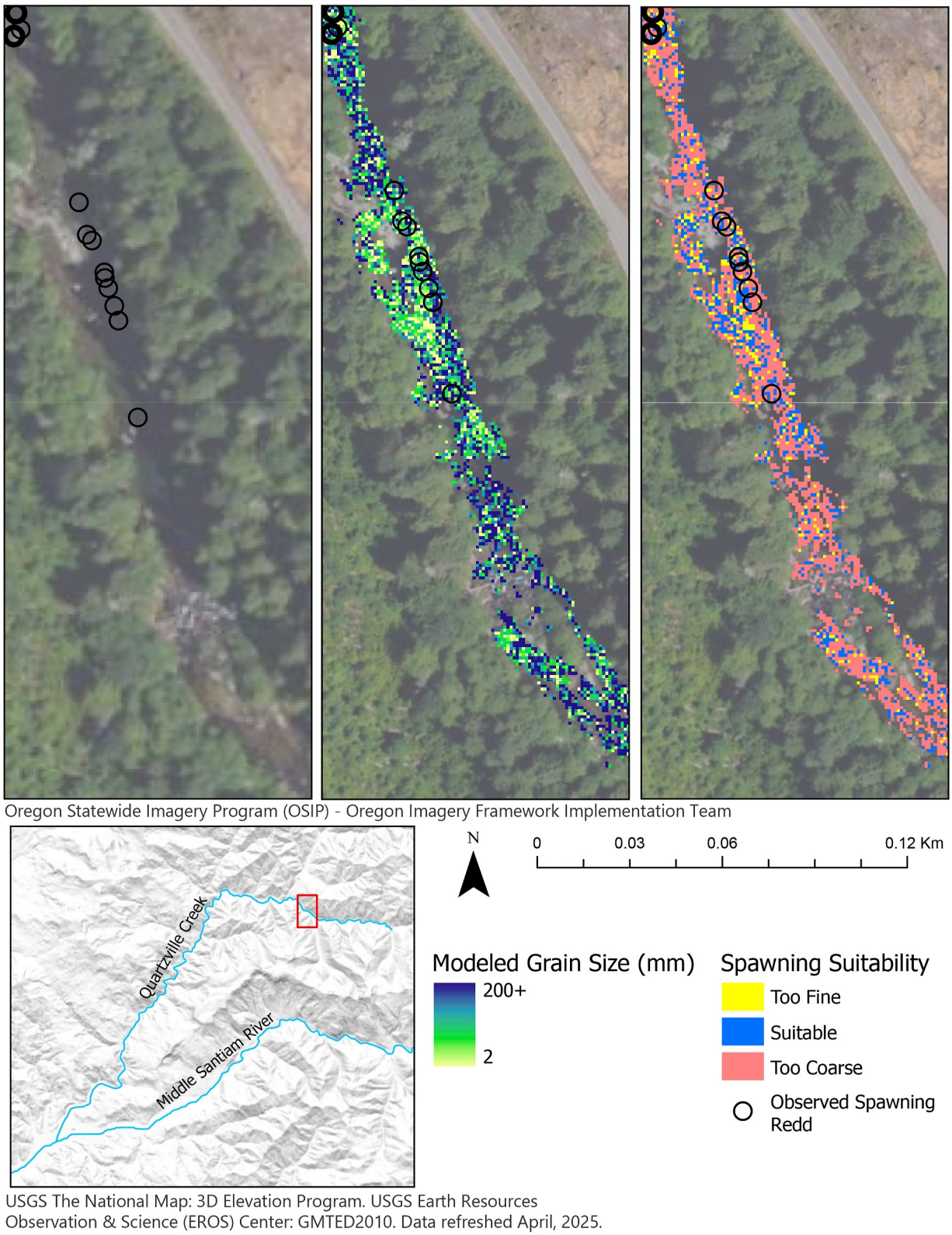

Figure 11. Modeled sediment size and spawning suitability on the unregulated Quartzville Creek.

also provide a solution in these more rugged reaches, particularly in short reaches. In the larger rivers where low point density is largely attributable to deeper water, lower flight elevations or stronger laser pulses might capture more of these areas, although in large rivers there will likely still be areas too deep for Lidar to measure. High density point clouds from multibeam sonar may be able to characterize grain sizes in such deep areas using a similar workflow as presented here with Lidar data.

Basin-wide analysis of D_{50} grain size facilitated sub-basin comparisons of GSDs, which also helps contextualize the available spawning sediment in each river. Aggregating GSD results in each basin shows that while there are similar grain size dynamics throughout much of the basin, there are notable intra-basin differences. For example, the upper South Santiam has a much larger percentage of finer-grained sediments compared the rest of the basin, while the upper North Santiam is has a larger percentage of coarse-grained sediments, particularly in the 100–200 mm range. These results can help inform broader geomorphological questions in the basin, such as the contribution and attrition of sediment within each basin.

Modeled D_{50} values were used to estimate the availability of suitable spawning sediment and compared against observed locations of Chinook salmon redds. Results show accurate identification of suitable spawning sediment in at least 70% of observed redd locations in all reaches surveyed, except the upper North Santiam River, where over half of the observed spawning locations were modeled as "too coarse." There are several potential reasons for this discrepancy, including over prediction of sediment size; GSDs changing between Lidar data collection and spawning; or that the maximum useable sediment size identified in the literature was too restrictive. The upper North Santiam had the strongest goodness-of-fit statistics of any study reach; however, it is unlikely that sediment model error alone is the sole factor in explaining the differences in spawning model fidelity. It's possible that geomorphic change from high flows occurred between Lidar collection (2023) and observed spawning (2024), however, given the proximity of the basins, any changes would likely be similar across reaches. While the suitable range of spawning gravels identified from the literature review may be too restrictive on the coarse range, as evidenced by the fact that about 25% of observed redds occurred in areas modeled as "too coarse," the use of a fixed range of suitable spawning sizes assumes that Chinook salmon use the same habitats throughout the watershed, which may not be the case.

One finding of this analysis was that suitable spawning sediments are distributed differently within the regulated and unregulated reaches that were studied. In the larger regulated reaches, suitable spawning sediments are often clustered in relatively large patches and interspersed with finer-grained sediments, while in the smaller unregulated streams, spawning sediment distribution was much patchier. This patchiness may have important implications for the capacity of these reaches to support salmon spawning given the fact that redd size scales with fish length and that Chinook salmon are large-bodied fish. Thurow (2000) documents that Chinook salmon required areas of 3–5 m^2, which is smaller than the 3–10 m^2 area reported by Riebe et al. (2014). No known data have been collected in the Santiam River Basin to inform the necessary area for redds and anecdotal observations from spawning observations noted that redd size varied between reaches. It is possible that some of the small patchy areas of suitable grain sizes are too small to support redd building and therefore it may be necessary to filter results by a threshold area prior to estimating spawning capacity.

Moreover, our prediction of grain size only reflects one component of spawning habitat and may not indicate the quantity of actual available spawning habitat, which is a function of many physical and biological drivers, such was channel hydraulics (Smith, 1973), water temperature (McCullough, 1999), and proximity to natal spawning grounds (Dittman & Quinn, 1996). Nevertheless, results from this analysis provide an upper limit on the potential available spawning habitat within the study extent. An important caveat is that the sediment models are not fully continuous, as low point density prohibited analysis in 9%–30% of the streambed area in the rivers studied. Further, the values used to assess sediment suitability for spawning were developed from a regional literature review, which can deviate significantly from locally used habitat. Collecting data on the sediment sizes used by spawning salmon in the study area would help to refine results and bolster confidence in the grain size models.

While the method presented to infer sediment size from Lidar point clouds is encouraging, this approach is unlikely to succeed in certain rivers. In particular, water turbidity can reduce Lidar penetration depth and subsequent accuracy. A common rule of thumb is that the maximum detectable depth of green wavelength Lidar is 1.5 times the Secchi depth (NV5 Geospatial, 2023). Thus, bathymetric Lidar data in highly turbid rivers will likely result in insufficient point densities for grain size analysis. Additionally, very shallow rivers or reaches of rivers might be difficult to capture, as there could be insufficient precision of both point classification and bathymetric

point correction to facilitate a reliable grain size analysis. For example, in very shallow water (less than ~0.03 m), it can be difficult to determine if a point has reflected from the bed, the water surface, or a protruding rock, and subsequent misclassification can reduce the accuracy of the water surface model used to correct for bed elevation. Finally, reaches with strong turbulence and entrainment of air will also likely have lower point densities, as photons are refracted by entrained air and the rough water surface can ultimately reduce the vertical accuracy of bathymetric points.

The coarse-grained, gravel- and cobble-bedded rivers evaluated in this study contain very little fine sediment on their channel beds, and thus the effect of fine sediment on grain size measurement from Lidar derived roughness is unknown. In particular, if significant amounts of fine sediment are present on the channel bed, such that interstitial spaces are filled by sands or smaller clasts, roughness will be reduced and may not be strongly correlated with measured coarse material on the streambed. Further, sand-bedded rivers, ripple and dune topography might dominate the roughness metrics, resulting in erroneous prediction of coarse grain sizes that, in turn, may falsely predict suitable spawning substrates. Finally, the largest grain sizes measured during pebble counts was typically 200–300 mm, though some were as large as 900 mm, and the paucity of large grains sampled results in higher uncertainty for these size classes. While the method presented in this paper could potentially be able to classify large sediment sizes, such as boulders, it is likely that this would require a larger kernel radius. Consequentially, there might be a limit of grain sizes that can be accurately captured using a single kernel value.

5. Conclusions

This study paired topo-bathymetric Lidar data with georeferenced pebble counts to model submerged surficial grain size along 260 km of river at 1 m^2 resolution. The study area included eight geomorphically distinct river reaches including reaches above and below high-head dams. The results of this analysis were then used to assess the availability of grain sizes suitable for spawning Chinook salmon. Findings show that standard topo-bathymetric Lidar was able to generate reasonably accurate estimates of measured grain size across a range of geomorphic conditions. Classifying predicted D_{50} values by sizes suitable for Chinook salmon spawning showed good agreement with observed redd locations, as well as substantial variation in how suitable spawning habitat is distributed in regulated and unregulated reaches. Such results can help inform management question such as how to distribute fish which have been transported above dams.

This approach to model grain size provides a means to map grain size at high resolution across large areas. This method can help to efficiently assess ecological and geomorphic conditions, such as available habitat or changes in grain size that might result from floods, wildfire, or dam removal, as well as informing fish-management questions, such as assessing potential for reintroduction in blocked or extirpated reaches, or restoration approaches and prioritization.

Acknowledgments
Any use of trade, firm, or product names is for descriptive purposes only and does not imply endorsement by the U.S. Government. This study was funded by the U.S. Geological Survey Next Generation Water Observing System (NGWOS) and the U.S. Army Corps of Engineers Portland District. Lidar collection was funded by the U.S. Geological Survey 3D Elevation Program (3DEP), U.S. Geological Survey NGWOS, and the U.S. Army Corps of Engineers Portland District. Authors acknowledge Max Schwid and Caelan Simeone for their assistance collecting pebble count data; Mikaeli Dirling, Will Long, Gabriel Hansen, and Brad Liedtke for their assistance collecting spawning data; Cindy Thatcher, Tom Carlson, Jeff Danielson, Paul Sclafani, and Marc Stewart for their assistance collecting Lidar data; and Jim O'Connor, Lee Harrison, Toby Kock, Carl Legleiter, Rose Wallick, and Mackenzie Keith for their insights into the study. Finally, authors thank peer reviewers for their insightful and constructive reviews of this manuscript. Their valuable feedback has significantly improved the quality of this work.

Data Availability Statement

Lidar data used in this analysis are available on The National Map Data downloader (https://www.apps.nationalmap.gov/datadownloader). Sediment model data are available on the USGS data clearing house, ScienceBase, https://doi.org/10.5066/P13SQVZY (White et al., 2025).

References

Bodine, C. S., Buscombe, D., & Hocking, T. D. (2024). Automated river substrate mapping from sonar imagery with machine learning. *Journal of Geophysical Research: Machine Learning and Computation*, *1*(3), e2024JH000135. https://doi.org/10.1029/2024JH000135

Bovee, K. D. (1982). *A guide to stream habitat analysis using the instream flow incremental methodology instream flow information Paper 12, FWS/OBS-82/26*. U. S. Fish and Wildlife Service, Office of Biological Services.

Brasington, J., Vericat, D., & Rychkov, I. (2012). Modeling river bed morphology, roughness, and surface sedimentology using high resolution terrestrial laser scanning. *Water Resources Research*, *48*(11), 2012WR012223. https://doi.org/10.1029/2012WR012223

Buffington, J. M., & Montgomery, D. R. (1999a). A procedure for classifying textural facies in gravel-bed rivers. *Water Resources Research*, *35*(6), 1903–1914. https://doi.org/10.1029/1999WR900041

Buffington, J. M., & Montgomery, D. R. (1999b). Effects of hydraulic roughness on surface textures of gravel-bed rivers. *Water Resources Research*, *35*(11), 3507–3521. https://doi.org/10.1029/1999WR900138

Buscombe, D. (2013). Transferable wavelet method for grain-size distribution from images of sediment surfaces and thin sections, and other natural granular patterns. *Sedimentology*, *60*(7), 1709–1732. Article 7. https://doi.org/10.1111/sed.12049

Buscombe, D. (2017). Shallow water benthic imaging and substrate characterization using recreational-grade sidescan-sonar. *Environmental Modelling and Software*, *89*, 1–18. https://doi.org/10.1016/j.envsoft.2016.12.003

Buscombe, D., & Masselink, G. (2009). Grain-size information from the statistical properties of digital images of sediment. *Sedimentology*, *56*(2), 421–438. Article 2. https://doi.org/10.1111/j.1365-3091.2008.00977.x

Buscombe, D., Rubin, D. M., & Warrick, J. A. (2010). A universal approximation of grain size from images of noncohesive sediment. *Journal of Geophysical Research*, *115*(F2), 2009JF001477. https://doi.org/10.1029/2009JF001477

Butler, J. B., Lane, S. N., & Chandler, J. H. (2001). Automated extraction of grain-size data from gravel surfaces using digital image processing. *Journal of Hydraulic Research*, *39*(5), 519–529. https://doi.org/10.1080/00221686.2001.9628276

Carbonneau, P. E., Bergeron, N., & Lane, S. N. (2005). Automated grain size measurements from airborne remote sensing for long profile measurements of fluvial grain sizes. *Water Resources Research*, *41*(11). Article 11. https://doi.org/10.1029/2005WR003994

Carbonneau, P. E., Lane, S. N., & Bergeron, N. E. (2004). Catchment-scale mapping of surface grain size in gravel bed rivers using airborne digital imagery. *Water Resources Research*, *40*(7). https://doi.org/10.1029/2003WR002759

Carrivick, J. L., & Smith, M. W. (2019). Fluvial and aquatic applications of Structure from Motion photogrammetry and unmanned aerial vehicle/drone technology. *WIREs Water*, *6*(1), e1328. https://doi.org/10.1002/wat2.1328

Chardon, V., Schmitt, L., Piégay, H., & Lague, D. (2020). Use of terrestrial photosieving and airborne topographic LiDAR to assess bed grain size in large rivers: A study on the Rhine River. *Earth Surface Processes and Landforms*, *45*(10), 2314–2330. https://doi.org/10.1002/esp.4882

CloudCompare (version 2.13.1). (2022). CloudCompare (version 2.13.1) [GPL software]. Retrieved from http://www.cloudcompare.org/

Dade, W. B. (2000). Grain size, sediment transport and alluvial channel pattern. *Geomorphology*, *35*(1–2), 119–126. https://doi.org/10.1016/S0169-555X(00)00030-1

Detert, M., Kadinski, L., & Weitbrecht, V. (2018). On the way to airborne gravelometry based on 3D spatial data derived from images. *International Journal of Sediment Research*, *33*(1), 84–92. https://doi.org/10.1016/j.ijsrc.2018.02.001

Detert, M., & Weitbrecht, V. (2012). Automatic object detection to analyze the geometry of gravel grains–A free stand-alone tool. *River flow 2012–Proceedings of the international conference on fluvial hydraulics* (Vol. 1, 595–600). https://doi.org/10.1201/b13250

Díaz Gómez, R., Pasternack, G. B., Guillon, H., Byrne, C. F., Schwindt, S., Larrieu, K. G., & Solis, S. S. (2022). Mapping subaerial sand-gravel-cobble fluvial sediment facies using airborne Lidar and machine learning. *Geomorphology*, *401*, 108106. https://doi.org/10.1016/j.geomorph.2021.108106

Dittman, A. H., & Quinn, T. P. (1996). Homing in pacific salmon: Mechanisms and ecological basis. *Journal of Experimental Biology*, *199*(1), 83–91. https://doi.org/10.1242/jeb.199.1.83

Duffin, J., Carmichael, R. A., Yager, E. M., Benjankar, R., & Tonina, D. (2021). Detecting multi-scale riverine topographic variability and its influence on Chinook salmon habitat selection. *Earth Surface Processes and Landforms*, *46*(5), 1026–1040. https://doi.org/10.1002/esp.5077

Duffin, J., Yager, E. M., Buffington, J. M., Benjankar, R., Borden, C., & Tonina, D. (2023). Impact of flow regulation on stream morphology and habitat quality distribution. *The Science of the Total Environment*, *878*, 163016. https://doi.org/10.1016/j.scitotenv.2023.163016

Erman, D. C., & Erman, N. A. (1984). The response of stream macroinvertebrates to substrate size and heterogeneity. *Hydrobiologia*, *108*(1), 75–82. https://doi.org/10.1007/BF02391635

Graham, D. J., Reid, I., & Rice, S. P. (2005). Automated sizing of coarse-grained sediments: Image-processing procedures. *Mathematical Geology*, *37*(1), 1–28. Article 1. https://doi.org/10.1007/s11004-005-8745-x

Greig, S. M., Sear, D. A., & Carling, P. A. (2005). The impact of fine sediment accumulation on the survival of incubating salmon progeny: Implications for sediment management. *The Science of the Total Environment*, *344*(1–3), 241–258. https://doi.org/10.1016/j.scitotenv.2005.02.010

Groom, J., Bertin, S., & Friedrich, H. (2018). Assessing intra-bar variations in grain roughness using close-range photogrammetry. *Journal of Sedimentary Research*, *88*(5), 555–567. https://doi.org/10.2110/jsr.2018.30

Heritage, G. L., & Milan, D. J. (2009). Terrestrial Laser Scanning of grain roughness in a gravel-bed river. *Geomorphology*, *113*(1–2), 4–11. https://doi.org/10.1016/j.geomorph.2009.03.021

Hiller, C., Leistner, S., Helfricht, K., & Achleitner, S. (2023). Robust estimations of areal grain size distribution from geometric surface roughness in a proglacial outwash area. *Geomorphology*, *439*, 108857. https://doi.org/10.1016/j.geomorph.2023.108857

Kinzel, P. J., Wright, C. W., Nelson, J. M., & Burman, A. R. (2007). Evaluation of an experimental LiDAR for surveying a shallow, braided, sand-bedded river. *Journal of Hydraulic Engineering*, *133*(7), 838–842. https://doi.org/10.1061/(asce)0733-9429(2007)133:7(838)

Kondolf, G. M., & Wolman, M. G. (1993). The sizes of salmonid spawning gravels. *Water Resources Research*, *29*(7), 2275–2285. https://doi.org/10.1029/93WR00402

Lamarche, G., Lurton, X., Verdier, A.-L., & Augustin, J.-M. (2011). Quantitative characterisation of seafloor substrate and bedforms using advanced processing of multibeam backscatter–Application to cook strait, New Zealand. *Continental Shelf Research*, *31*(2), S93–S109. https://doi.org/10.1016/j.csr.2010.06.001

McCullough, D. A. (1999). *A review and synthesis of effects of alterations to the water temperature regime on freshwater life stages of salmonids, with special reference to Chinook salmon*. US EPA. Water Resources Assessment, 910-R-99-010. (p. 291).

McKean, J., Nagel, D., Tonina, D., Bailey, P., Wright, C. W., Bohn, C., & Nayegandhi, A. (2009). Remote sensing of channels and riparian zones with a narrow-beam aquatic-terrestrial LIDAR. *Remote Sensing*, *1*(4), 1065–1096. https://doi.org/10.3390/rs1041065

McKean, J. A., Isaak, D. J., & Wright, C. W. (2008). Geomorphic controls on salmon nesting patterns described by a new, narrow-beam terrestrial–aquatic Lidar. *Frontiers in Ecology and the Environment*, *6*(3), 125–130. https://doi.org/10.1890/070109

McNeil, W. J., & Ahnell, W. H. (1964). *Success of pink salmon spawning relative to size of spawning bed materials*. US Department of the Interior, Bureau of Commercial Fisheries.

Montgomery, D. R., Buffington, J. M., Peterson, N. P., Schuett-Hames, D., & Quinn, T. P. (1996). Stream-bed scour, egg burial depths, and the influence of salmonid spawning on bed surface mobility and embryo survival. *Canadian Journal of Fisheries and Aquatic Sciences*, *53*(5), 1061–1070. https://doi.org/10.1139/f96-028

National Oceanic and Atmospheric Administration (NOAA). (2021). Endangered Species Act threatened and endangered species directory. Retrieved from https://www.fisheries.noaa.gov/species-directory/threatened-endangered

Neverman, A. J., Fuller, I. C., Procter, J. N., & Death, R. G. (2019). Terrestrial laser scanning and structure-from-motion photogrammetry concordance analysis for describing the surface layer of gravel beds. *Progress in Physical Geography: Earth and Environment*, *43*(2), 260–281. https://doi.org/10.1177/0309133318822966

NV5 Geospatial. (2023). 2023 topobathymetric Lidar technical data report, Santiam River, Oregon (Technical Data Report No. 300122) (p. 47).

O'Connor, J. E., Mangano, J. F., Anderson, S. W., Wallick, J. R., Jones, K. L., & Keith, M. K. (2014). Geologic and physiographic controls on bed-material yield, transport, and channel morphology for alluvial and bedrock rivers, western Oregon. *Geological Society of America Bulletin*, *126*(3–4), 377–397. https://doi.org/10.1130/B30831.1

Pebesma, E. (2018). Simple features for R: Standardized support for spatial vector data. *The R Journal*, *10*(1), 439. https://doi.org/10.32614/RJ-2018-009

Purinton, B., & Bookhagen, B. (2019). Introducing PebbleCounts: A grain-sizing tool for photo surveys of dynamic gravel-bed rivers. *Earth Surface Dynamics*, *7*(3), 859–877. Article 3. https://doi.org/10.5194/esurf-7-859-2019

R Core Team. (2024). *_R: A language and environment for statistical computing_*. R Foundation for Statistical Computing. Retrieved from https://www.R-project.org/

Riebe, C. S., Sklar, L. S., Overstreet, B. T., & Wooster, J. K. (2014). Optimal reproduction in salmon spawning substrates linked to grain size and fish length. *Water Resources Research*, *50*(2), 898–918. https://doi.org/10.1002/2013WR014231

Roussel, J.-R., Auty, D., Coops, N. C., Tompalski, P., Goodbody, T. R. H., Meador, A. S., et al. (2020). lidR: An R package for analysis of Airborne Laser Scanning (ALS) data. *Remote Sensing of Environment*, *251*, 112061. https://doi.org/10.1016/j.rse.2020.112061

Rubin, D. M. (2004). A simple autocorrelation algorithm for determining grain size from digital images of sediment. *Journal of Sedimentary Research*, *74*(1), 160–165. https://doi.org/10.1306/052203740160

Schneck, F., Schwarzbold, A., & Melo, A. S. (2011). Substrate roughness affects stream benthic algal diversity, assemblage composition, and nestedness. *Journal of the North American Benthological Society*, *30*(4), 1049–1056. https://doi.org/10.1899/11-044.1

Sime, L. C., & Ferguson, R. I. (2003). Information on grain sizes in gravel-bed rivers by automated image analysis. *Journal of Sedimentary Research*, *73*(4), 630–636. https://doi.org/10.1306/112102730630

Smith, A. K. (1973). Development and application of spawning velocity and depth criteria for Oregon salmonids. *Transactions of the American Fisheries Society*, *102*(2), 312–316. https://doi.org/10.1577/1548-8659(1973)102<312:DAAOSV>2.0.CO;2

Storz-Peretz, Y., & Laronne, J. B. (2013). Morphotextural characterization of dryland braided channels. *Geological Society of America Bulletin*, *125*(9–10), 1599–1617. https://doi.org/10.1130/B30773.1

Tague, C., & Grant, G. E. (2004). A geological framework for interpreting the low-flow regimes of Cascade streams, Willamette River Basin, Oregon. *Water Resources Research*, *40*(4), W04303. https://doi.org/10.1029/2003WR002629

The Interagency Working Group on Ocean and Coastal Mapping. (2018). National coastal mapping strategy 1.0: Costal LIDAR elevation for a 3D nation. Retrieved from https://iocm.noaa.gov/about/documents/strategic-plans/IWG-OCM-Final-Coastal-Mapping-Strategy-2018-with-cover.pdf

Thurow, R. F. (2000). Dynamics of chinook salmon populations within Idaho's Frank Church Wilderness: Implications for persistence. In S. F. McCool, D. N. Cole, W. T. Borrie, & J. O'Loughlin (Eds.), *Wilderness science in a time of change, proceedings RMRS-P-15-VOL-3* (pp. 143–151). USDA Forest Service, Rocky Mountain Research Station.

Tiffan, K. F., Garland, R. D., & Rondorf, D. W. (2002). Quantifying flow-dependent changes in subyearling fall chinook salmon rearing habitat using two-dimensional spatially explicit modeling. *North American Journal of Fisheries Management*, *22*(3), 713–726. https://doi.org/10.1577/1548-8675(2002)022<0713:QFDCIS>2.0.CO;2

Tonina, D., & Buffington, J. M. (2009). Hyporheic exchange in mountain rivers I: Mechanics and environmental effects. *Geography Compass*, *3*, 1063–1086. https://doi.org/10.1111/j.1749-8198.2009.00226.x

U.S. Geological Survey. (2024). 3D elevation Program Lidar point cloud. (published 20241003), Retrieved from https://www.usgs.gov/tools/download-data-maps-national-map

Vázquez-Tarrío, D., Borgniet, L., Liébault, F., & Recking, A. (2017). Using UAS optical imagery and SfM photogrammetry to characterize the surface grain size of gravel bars in a braided river (Vénéon River, French Alps). *Geomorphology*, *285*, 94–105. https://doi.org/10.1016/j.geomorph.2017.01.039

Warrick, J. A., Rubin, D. M., Ruggiero, P., Harney, J. N., Draut, A. E., & Buscombe, D. (2009). Cobble cam: Grain-size measurements of sand to boulder from digital photographs and autocorrelation analyses. *Earth Surface Processes and Landforms*, *34*(13), 1811–1821. Article 13. https://doi.org/10.1002/esp.1877

White, J. S., Bartelt, K. M., & Overstreet, B. T. (2025). Submerged grain size maps in the Santiam River Basin, Oregon. *U.S. Geological Survey data release*. https://doi.org/10.5066/P13SQVZY

Wolman, G. M. (1954). A method of sampling coarse river-bed material. *Eos, Transactions American Geophysical Union*, *35*(6), 951–956. https://doi.org/10.1029/TR035i006p00951

Woodget, A. S., & Austrums, R. (2017). Subaerial gravel size measurement using topographic data derived from a UAV-SfM approach. *Earth Surface Processes and Landforms*, *42*(9), 1434–1443. https://doi.org/10.1002/esp.4139